

Introduction to Higher Order Spatial Statistics in Cosmology

István Szapudi¹

Institute for Astronomy, University of Hawaii,
2680 Woodlawn Dr, Honolulu, HI 96822
szapudi@ifa.hawaii.edu

1 Introduction

Higher order spatial statistics characterize non-Gaussian aspects of random fields, which are ubiquitous in cosmology: from the Cosmic Microwave Background (CMB) to the large scale structure (LSS) of the universe. These random fields are rich in their properties; they can be continuous or discrete; can have one through three, or even more dimensions; their degree of non-Gaussianity ranges from tiny to significant. Yet, there are several techniques and ideas, which are applicable to virtually all cosmological random fields, be it Lyman- α forests, LSS, or CMB.

In this lecture notes I concentrate on the classic and widely applicable characterization of higher order statistics by joint moments, a.k.a. higher order correlation functions, and directly related statistics. These statistics are very powerful, although have a perturbative nature to them in that they constitute an infinite (formal) expansion. Clearly, when only the first N terms of this expansion are extracted from data, interesting information might remain in even higher order terms. This is why a host of alternative statistics (void probabilities, wavelets, Minkowski-functionals, minimal spanning trees, phase correlations, etc. just to name a few) are introduced and used extensively in the literature, in complementary fashion to N -point functions. More on these alternatives appear in other lecture notes of this volume, and if your appetite is whet you should read e.g., [1] for more information. The present lecture notes serve as an informal introduction to the subject, a starting point for further studies, rather than a full-blown review.

Higher order statistics are complicated due to several factors. Most of them arise from the large configuration space of parameters which results in a “combinatorial explosion” of terms. For instance, the first non-trivial 3-point correlation function can in principle depend on 9 coordinates. Taking into account applicable symmetries still leaves 3 parameters in real space, and 6 parameters in redshift space (5 if one uses the distant observer approximation). This dependence on a large number of parameters renders higher order statistics quite cumbersome, their measurement, interpretation and visualization surprisingly complex and CPU intensive. For the same reason, theoretical prediction of higher order statistics correspondingly involved, non-linearities, redshift distortions or projection effects, and bias affect them in subtle and

non-trivial ways. In addition, higher order statistics are more sensitive to geometry and systematics than their low order cousin, the two-point correlation function. This means that a comparatively larger and cleaner sample is needed for effective studies. Even with the presently available large surveys, such as SDSS and 2dF, the overlap between well understood theory and reliable measurement is in fact disquietingly small.

Despite the above difficulties, the study of higher order statistics is a rewarding one, both intellectually and scientifically. The simple idea that small initial fluctuations grew by gravitational amplification is enough to predict higher order correlation functions, at least on large scales, to impressive accuracy. Analytical predictions and simulations contrasted with data have already provided a strong support for Gaussian initial conditions, and show that our basic picture of structure formation is correct.

On the other hand, the two-point correlation function alone gives a quite simplistic view of LSS, which has been visually demonstrated first by Alex Szalay, through randomizing the phases of a highly non-Gaussian simulation. This procedure erases a large portion of (although not all) higher order correlations, while keeping the two-point statistics (c.f. Fig. 1. in Peter Coles' lecture notes in the same volume). It is striking how most structure we see in the simulation disappears when higher order information is erased, despite that the two-point function (or power spectrum) is the same.

In addition, the two-point correlation function is degenerate with respect to the bias (the difference between the statistics of the observed “light” from galaxies and the underlying dark matter), and the amplitude of primordial fluctuations. Most methods which extract information from the two-point correlation function or power spectrum alone, draw on assumptions about the bias to avoid this degeneracy problem, and/or combine with CMB measurements. Higher order statistics not only yields a more accurate picture of the distribution, but resolves the degeneracy of the two-point function by constraining the bias.

These notes focus on phenomenological aspects of higher order correlation functions and related statistics. In particular, I emphasize the relationship of these statistics with symmetries. Some aspects of this are quite new, and it is the only way I know how to ease the pain of the above mentioned “combinatorial explosion”, at least partially. In the next sections I review the most important theoretical and statistical information, in particular I present the definitions of the statistics, estimators, how errors are calculated, algorithms to realize the estimators, and some points on bias, redshift distortions. I develop symmetry considerations in slightly more detail throughout. For completeness, I include the foundations of perturbation theory; a detailed recent review is available by [2] which is highly recommended. Finally, I illustrate most of the above through an example by working out the theory of conditional cumulants. Finally, while LSS is emphasized in examples, most of the theory is directly applicable to CMB, or any other random field as well.

2 Basic Definitions

The learning curve of higher order statistics is initially steep, partly due to the large number of new concepts and definitions which need to be absorbed. Here I attempt to collect some of the most basic definitions which will be used later.

Spatial Random Field A is field which has random values at all spatial points. Its corresponding measure is a functional, $\mathcal{P}(A)\mathcal{D}A$, the “probability” of a realization. This is analogous to a probability density. Averages can be calculated via functional integrals, which although not always well defined mathematically, are very pictorial.

Ensemble Average We denote with $\langle A \rangle$ the ensemble average of some quantity A . The averaging corresponds to a functional integral over the density measure. Physically this means simply the average of the quantity over infinite (or many) independent realizations.

Ergodicity In the study of random fields it is often assumed that ensemble averages can be replaced with spatial averages. Physically this means that distant parts of the random field are uncorrelated, and thus a large realization of the random field (a “representative volume”, hopefully the chunk of our universe which is observable) can be used for measurements of statistical quantities.

Joint Moments The most basic set of statistics we can consider to characterize a random field T are the joint moments of the field taken at N distinct points x_1, \dots, x_N ,

$$F^{(N)}(x_1, \dots, x_N) = \langle T(x_1), \dots, T(x_N) \rangle \quad (1)$$

We often work with fluctuation fields which have been normalized with the average: $\delta = \frac{T}{\langle T \rangle} - 1$. Note that the spatial dependence on coordinate x_i is often abbreviated as δ_i . No assumption is made on the dimensionality of the random field. One (Lyman alpha forest), two (CMB, LSS projected catalogs), or three (LSS redshift surveys) dimensional fields are typical in cosmology.

Connected Moments Connected moments are denoted with $\langle \rangle_c$ and are defined recursively with the following formula:

$$\langle \delta_1, \dots, \delta_N \rangle_c = \langle \delta_1, \dots, \delta_N \rangle - \sum_P \langle \delta_1 \dots \delta_i \rangle_c \dots \langle \delta_j \dots \delta_k \rangle_c \dots, \quad (2)$$

where P denotes symbolically a summation of all possible partitions. In other words, connected moment of all possible partitions have to be subtracted from the full (or disconnected) joint moment. What is left is the connected moment.

N-point correlation functions are defined as the connected joint moments of the normalized fluctuation field δ

$$\xi^{(N)}(1, \dots, N) = \langle \delta_1, \dots, \delta_N \rangle_c, \quad (3)$$

where we introduce yet another short hand for denoting $\xi^N(x_1, \dots, x_N)$. The three-point correlation function is often denoted with ζ instead of $\xi^{(3)}$, and the two-point correlation function with $\xi \equiv \xi^{(2)}$. Most statistics we are dealing with in this review are special cases of N -point correlation functions.

Gaussian A random field is called Gaussian if its first and second moments fully determine it statistically. We will often use the field δ , which denotes a random field whose average is 0. Then a Gaussian field is fully determined by its two-point correlation function $\xi = \langle \delta_1 \delta_2 \rangle$. Gaussian random fields have trivial higher order moments in that all their connected moments vanish for $N \geq 3$ (Wick-theorem).

Non-Gaussian A non-Gaussian field has at least one non-vanishing higher than second connected moment. Note that the definition of non-Gaussian is highly general (like “non-Elephant”) everything what is not Gaussian is non-Gaussian. Therein lies one of the highest difficulty of the subject.

Cumulants correspond to the simplest special case of N -point functions: the joint moment of a degenerate configuration, where all the field values are taken at the same place. The usual definition in cosmology is

$$S_N = \frac{\langle \delta^N \rangle_c}{\langle \delta^2 \rangle^{N-1}}, \quad (4)$$

where the normalization with the average correlation function $\bar{\xi} = \langle \delta^2 \rangle$ is motivated by the dynamics of perturbation theory. Other normalizations might be more suitable, e.g., for CMB. Cumulants depend only on one scale: the smoothing kernel of δ which implicit in the above equation. This fact accounts for most of their popularity, and indeed they are the only statistics (along with cumulant correlators), which have been measured as high order as $N = 10$ for galaxies. An alternative definition is $Q_N = S_N / N^{N-2}$, which corresponds to the division with the number of possible trees graphs. This definition typically ensures that for galaxies and dark matter all Q_N 's are of order unity.

Cumulant Correlators correspond to the next simplest special case of $N + M$ -point functions: the joint moment of a doubly degenerate configuration, where the N and M field values are taken at two places, respectively. The usual definition in cosmology is

$$Q_{N,M} = \frac{\langle \delta_1^N \delta_2^M \rangle_c}{\langle \delta^2 \rangle^{N+M-1} \langle \delta_1 \delta_2 \rangle^{N-2} M^{M-2}}. \quad (5)$$

Other generalizations, e.g. with triple degeneracy, are obvious, but not clear whether fruitful. In the above, it is assumed that the smoothing kernel is the same for both points, which is usual, although not necessary. When the normalization of the possible number of trees is not done, the quantity is often denoted with $C_{N,M}$.

Conditional Cumulants are defined as the joint connected moment of one unsmoothed and $N - 1$ smoothed density fluctuation fields. They can be real-

ized by integrals of the N -point correlation function through $N - 1$ spherical top-hat windows,

$$U_N(R_1, \dots, R_{N-1}) = \int \xi_N(x_1, \dots, x_{N-1}, 0) \prod_{i=1}^{N-1} d^3 x_i \frac{W_{R_i}(x_i)}{V_i} \quad (6)$$

where $V_i = 4\pi/3R_i^3$ is the volume of the window function W_{R_i} . In the most general case, each top hat window might have a different radius. The conditional cumulants are analogous to ordinary cumulants, but subtly different: they have an advantageous smoothing kernel which enables their measurement with an edge corrected estimator (more on this later).

Power Spectrum Since space is assumed to be *statistically* invariant under translations, it is convenient to introduce the Fourier transform of the D -dimensional field

$$\delta(x) = \int \frac{d^D k}{(2\pi)^D} \delta_k e^{ikx}. \quad (7)$$

The translation invariance causes the independent k -modes to be uncorrelated, which renders the correlation function of the Fourier modes “diagonal”

$$\langle \delta_{k_1} \delta_{k_2} \rangle \equiv \delta_D(k_1 + k_2) (2\pi)^D P(k), \quad (8)$$

which is the definition of the power spectrum. (δ_D is the Dirac- δ function.) It can be shown that the power spectrum is the Fourier transform of the two-point correlation function ξ . Note that the $(2\pi)^D$ normalization is customary, but it is not followed by everybody.

Poly-Spectra Similarly to the power spectrum, the joint connected moments of N -Fourier modes are called a poly-spectra ($N - 1$ -spectrum) modulo a Dirac- δ function. The most important special case is the bispectrum, the Fourier transform of the three-point correlation function $\zeta \equiv \xi^{(3)}$. The next order is called tri-spectrum.

A Discrete Random Field corresponds to all possible arrangements of discrete objects (whose number can also vary) with the corresponding measure. A generalization over the continuous random field which is needed to describe the statistics of the distribution objects in space, such as galaxies.

Poisson Sampling Often it is a good approximation to derive a discrete random field from a continuous one via a simple assumption: take an infinitesimally small volume, such that the probability of having more than one object in the volume is negligible, and simply assume that the probability of having one object is proportional to the value of the field within the small volume. This is called an infinitesimal Poisson process.

Discreteness Effects correspond to the difference between the statistics of an observed, discrete random field and an assumed underlying, continuous random field. Also known as shot noise, or Poisson noise. It can be especially simply calculated under the assumption of infinitesimal Poisson sampling.

3 Estimators

The main idea underlying the construction of estimators for spatial statistics is the ergodic theorem. If we replace the ensemble averages with spatial averages, we obtain estimators for the above defined quantities.

To put the above simple idea into practice, one has to deal with some subtleties as well. I list a few interesting ones: discreteness, counts in cells, edge correction, and optimality.

3.1 Discreteness

Imagine a galaxy catalog with average count \bar{N} in a given cell of size R , our chosen smoothing length. We can estimate approximately the density at each cell as $\tilde{\delta}_i \simeq \frac{N_i}{\bar{N}} - 1$. The above simple idea suggest to estimate the K -th order cumulant with (for a quantity A we denote its estimator \tilde{A} throughout).

$$\tilde{S}_K \propto \frac{1}{N_{tot}} \sum \tilde{\delta}_i^K |_c. \quad (9)$$

A little more thought, however, reveals that, while our estimator for density field is unbiased, our estimator for the cumulant is not. While $\langle N \rangle = \bar{N} \langle 1 + \delta \rangle = \bar{N}$, $\langle N^K \rangle \neq \bar{N}^K \langle (1 + \delta)^K \rangle$. The reason for this is the “self contribution” to correlations, a typical discreteness effect.

To see this, let’s follow [3], and imagine for $K = 2$ that our cell of size R is divided into T infinitesimally small cells, each of them small enough that the probability of having more than one galaxy in it would be negligible. Let’s call the number of galaxies in each tiny cells μ_i . Since $\mu_i = 0, 1$, $\mu_i^K = \mu_i$ for any K . This means that all moments $\langle \mu_i^K \rangle = \langle \mu_i \rangle = \bar{N}/T$. The total number of objects in our original cell is $\sum \mu_i$. Now it is easy to see that

$$\langle N^2 \rangle = \left(\sum \mu_i \right)^2 = \sum_i \langle \mu_i \rangle + \sum_{i \neq j} \langle \mu_i \rangle \langle \mu_j \rangle (1 + \xi_{ij}), \quad (10)$$

With $T \rightarrow \infty$ the above expression yields the final results

$$\begin{aligned} \langle N^2 \rangle &= \bar{N} + \bar{N}^2 (1 + \bar{\xi}) \\ &= \bar{N} + \bar{N}^2 \langle (1 + \delta)^2 \rangle. \end{aligned} \quad (11)$$

The first term corresponds to the Poisson-noise bias of our estimator. Note that we already simplified the case assuming that \bar{N} and all the normalization required to obtain S_K from the above is known a priori.

Higher orders can be calculated either with the above suggestive, but tedious method, or with generating functions one can prove the following simple rule [4]

$$\langle (N)_K \rangle = \bar{N}^K \langle (1 + \delta)^K \rangle, \quad (12)$$

where $\langle(N)_K\rangle = \langle N(N-1)\cdots(N-K+1)\rangle$ are the factorial moments of N (the quantity inside the average is called falling factorial). In other words, if you replace regular moments with factorial moments, discreteness effects magically disappear. With this simple rule, and taking into account that discreteness can only affect overlap, you can construct estimators free from discreteness biases for any of our defined estimators. E.g.

$$\begin{aligned}\langle(N)_2\rangle &= \bar{N}^2(1 + \bar{\xi}) \\ \langle(N)_3\rangle &= \bar{N}^3\langle(1 + 3\delta + 3\delta^2 + \delta^3)\rangle \\ &= \bar{N}^3(1 + 3\bar{\xi} + 3S_3\bar{\xi}^2)\end{aligned}\tag{13}$$

and all you have to do is express algebraically S_3 as a function of the factorial moments. It is a good exercise, for solutions see [5].

Note that both intuition and halo models [6] suggest that Poisson sampling might not be a good approximation on very small scales for galaxy surveys. When in doubt (i.e. no well defined and trusted model for the discreteness exist), try to use estimators without self-overlap, since discreteness manifests itself through self-correlations only.

3.2 Counts in Cells

We have shown in the previous subsection how to construct estimators for cumulants, cumulant correlators, etc. even in the discrete case. For cumulants, however, a more efficient method exists based on counts in cells.

According to the previous subsection, if we can estimate factorial moments $\langle(N)_K\rangle$, it is a simple matter of calculation to obtain cumulants. While one could directly estimate the factorial moments from data, the usual procedure is to estimate first the probability P_N that a cell of a given volume (or area) contains N objects. Then the factorial moments can be calculated as

$$\langle(N)_K\rangle = \sum_{N\geq 0} P_N(N)_K.\tag{14}$$

The advantage of this technique is that there exist many fast and efficient algorithms to estimate P_N from data, and once the counts in cells probabilities are estimated, arbitrary high order cumulants can be obtained in a straightforward manner.

3.3 Edge Correction and Heuristic Weights

If signal and noise were uniform, uniform weighting of objects would be optimal as required by symmetry. On scales approaching the characteristic size of a survey, uneven (or more generally suboptimal) weighting of objects near the edges of the survey will often dominate the errors. The optimal weight has contributions from survey geometry and correlations (signal and noise),

and it is not even diagonal. These two effects are only separate conceptually, but they are often coupled in non-trivial ways.

Edge correction with heuristic weights fully accounts for the effect of survey geometry (including uneven sampling, etc), however, it does not include a prior on the correlations. For instance, the heuristic weights used in the SpICE method [7] are exact in the noise dominated regime, however, they are only approximate when the signal is important.

A class of edge corrected estimators [10, 11] can be written symbolically as

$$\tilde{\xi}^N = \sum_{i_1, \dots, i_N} w_{i_1, \dots, i_N} (\delta_{i_1} \dots \delta_{i_N})_c \quad (15)$$

which is formally the same as the quantity we want to measure, except we replace $\langle \rangle$ with an average over the sample itself according to the ergodic principle. The heuristic weights are such that their total sum is 1, and usually correspond to an inverse variance. This would be exact if the bins were uncorrelated, which is usually not the case. It can be a good approximation power spectra as shown by [8] (c.f. lecture notes of Andrew Hamilton in this volume).

Note that above estimator introduce additional subtleties due to taking of connected moments, and due to the non-linear nature of the estimator. The non-linearity is introduced by calculating the fluctuations via a division with the average density. If we estimate the average density from the same sample, the bias due to this effect is termed the “integral constraint”.

In practice, the above estimator is often replaced with a Monte Carlo version ([9] for the two-point correlation function, and [10, 11] for the N -point functions). Let D , and R denote the data set, and a random set, respectively. The latter is a random distribution over the geometry and sampling variations in the survey. If we define symbolically an estimator $D^p R^q$, with $p + q = N$ for a function Φ symmetric in its arguments

$$D^p R^q = \sum \Phi(x_1, \dots, x_p, y_1, \dots, y_q), \quad (16)$$

with $x_i \neq x_j \in D, y_i \neq y_j \in R$. As an example, the two point correlation function corresponds to $\Phi(x, y) = [x, y \in D, r \leq d(x, y) \leq r + dr]$, where $d(x, y)$ is the distance between the two points, and $[condition]$ equals 1 when $condition$ holds, 0 otherwise.

The estimator for the N -point correlation functions is written with the above symbolic notation as $(\hat{D} - \hat{R})^N$, or more precisely,

$$\tilde{\xi}_N = \frac{1}{S} \sum_i \binom{N}{i} (-)^{N-i} \left(\frac{D}{\lambda}\right)^i \left(\frac{R}{\rho}\right)^{N-i}, \quad (17)$$

where $S = \int \Phi \mu_N$, a simple phase space integral, and λ, ρ are the densities of data and random sets. (for details see [11]). This is the Monte Carlo version of the edge corrected estimator.

It is worthwhile to note is that counts in cells cannot be properly edge corrected, although approximate procedures exist in the regime where the probabilities have a weak dependence on the cell shape, or one could integrate the above estimators numerically.

3.4 Optimality

For the measurement of the two-point function for a Gaussian process we know that maximum likelihood methods are optimal in the sense that no other method can achieve smaller variance. This can be shown with the use of the Fisher matrix and the Cramer Rao inequality [12, 13] (see also the lecture notes of Andrew Hamilton in this volume) Since our previous prescription for edge effects is different (in particular it does not know about correlations), it is clearly suboptimal. Given that we know the optimal method, why don't we use it for all measurements? The reason is that there are caveats, which, especially for galaxy surveys, severely limit the applicability (and optimality) of the optimal method.

- Computational issues: The quadratic incarnation of the maximum likelihood method for two-point correlation function (or power spectrum) amounts to sandwiching the projection matrix $P_l = \partial C / \partial l$, the derivative of the full (signal plus noise) correlation matrix according to the l -th parameter C_l between the data vectors weighted by the inverse correlation matrix C^{-1} , yielding

$$\tilde{C}_l = \langle C^{-1} x | P_l | C^{-1} x \rangle, \quad (18)$$

where \tilde{C}_l is the estimator for C_l . We can see from this that the inverse of the correlation matrix needs to be calculated, which typically scales as $O(N^3)$ with the number of data items¹. For $N \simeq 1000$ this can be done on a laptop computer (about 17 sec on mine), but for $N \gtrsim 10^6$ it becomes prohibitive even for the fastest supercomputers (not to mention storage capacity, which might also become unrealistic for a large data set). Iterative, and brute force maximum likelihood methods, although seemingly more complicated, scale the same way.

State of the art data sets (“mega-pixel” CMB maps, such as WMAP and Planck, as well as decent LSS surveys) are way beyond present day computational capabilities (unless some special tricks and approximations are involved, e.g., [14]).

- Caveats: the “lossless and optimal” property of the maximum likelihood estimator is subject to practical limitations. Data reduction and analysis involve many subtle choices, such as systematic corrections, binning,

¹There are methods, such as preconditioned conjugate gradients, with which $C^{-1}x$ can be calculated in $O(N^2)$. However, the Fisher matrix still needs $O(N^3)$ computations

- pixellization, etc. In the past these turned into differences between analyses which all used the same optimal method. In addition, non-iterative quadratic maximum likelihood estimators are posteriors based on a prior, thus they are only optimal in the limit when we have full prior knowledge of what we want to measure.
- The Gaussianity condition: while it is an excellent approximation for the CMB, it breaks down for the LSS even on very large scales. In the Bayesian sense, the Gaussian prior is not justified, thus the estimators might become sub-optimal, and might even be biased. Those measurements, where variants of the maximum likelihood are method are used for LSS, take great pain at controlling “non-linear contamination”, e.g. with filtering. Besides the computational aspects, this is the main reason why many LSS analyses still use heuristic weights. However, some aspects of the maximum likelihood method have been adapted to deal with non-Gaussianities [15], and even for estimating three-point correlation functions under the assumption of Gaussianity [16, 17] (this is not a contradiction: when the non-Gaussianity is tiny, as in CMB, correlation matrices can be well approximated with a Gaussian assumption).

4 Errors

The formal calculation of errors (or more generally covariance matrices) is straightforward from Equation 15: one simply takes the square of the equation and performs ensemble averages. In general, for two bins represented by the weights w^a and w^b , the errors will scale as

$$\Delta \tilde{\xi}^N = \sum_{i_1, \dots, i_N} w_{i_1, \dots, i_N}^a w_{j_1, \dots, j_N}^b \langle \delta_{i_1} \dots \delta_{i_N} \delta_{j_1} \dots \delta_{j_N} \rangle. \quad (19)$$

In practice, complications will arise from i) the large number of terms ii) the complicated summation (or integral in the continuum limit) iii) the overlaps between indices and the corresponding discreteness terms iv) the theoretical expression of the ensemble averages. However, we can draw the general idea from the expression that the covariance matrix of N -point estimators depends on $2N$ -point correlation functions. Next we demonstrate this formula with the calculation of the errors on the two-point correlation function.

To specify more our symbolic estimator, let us assume that the survey is divided into K pixels, each of them with fluctuations δ_i , with i running from $1 \dots K$. For this configuration our estimator can be written as

$$\tilde{\xi} = w_{12} \delta_1 \delta_2. \quad (20)$$

The above equation uses a “shorthand” Einstein convention: 1, 2 substituting for i_1, i_2 , and repeated indices summed, and it is assumed that the two indices cannot overlap.

The ensemble average of the above estimator is clearly $w_{12}\xi_{12}$. The continuum limit (co)variance between bins a and b can be calculated by taking the square of the above, and taking the ensemble average.

$$\langle \delta\tilde{\xi}^a \delta\tilde{\xi}^b \rangle = w_{12}^a w_{34}^b (\langle \delta_1 \delta_2 \delta_3 \delta_4 \rangle - \langle \delta_1 \delta_2 \rangle \langle \delta_3 \delta_4 \rangle). \quad (21)$$

Note that the averages in this formula are not connected moments, which are distinguished by $\langle \rangle_c$.

The above equation yields only the continuum limit terms. To add Poisson noise contribution to the error, note that it arises from the possible overlaps between the indices (indices between two pairweights *can* still overlap!). In the spirit of infinitesimal Poisson models, we replace each overlap with a $1/\lambda$ term, and express the results in terms of connected moments. There are three possibilities, i) no overlap (continuum limit)

$$w_{12}^a w_{34}^b (\xi_{1234} + \xi_{13\xi_{24}} + \xi_{14\xi_{23}}), \quad (22)$$

ii) one overlap (4 possibilities)

$$\frac{4}{\lambda} w_{12}^a w_{13}^b (\xi_{123} + \xi_{23}), \quad (23)$$

iii) two overlaps (2 possibilities)

$$\frac{2}{\lambda^2} w_{12}^a w_{12}^b (1 + \xi_{12}), \quad (24)$$

In these equations, for the sake of the Einstein convention we used $\xi(i, j, k, l) \rightarrow \xi_{ijkl}$. The above substitutions (rigorously true only in the infinitesimal Poisson sampling limit) become increasingly accurate with decreasing cell size. For the Monte Carlo estimator of Eq. 17 a slightly more general formula is valid, where the summation is replaced with integrals over a bin function $\Phi(1, 2)$

$$\begin{aligned} \langle \delta\tilde{\xi}_2^a \delta\tilde{\xi}_2^b \rangle &= \frac{1}{S^2} \left\{ \int \Phi_a(1, 2) \Phi_b(3, 4) [\xi_4(1, 2, 3, 4) + 2\xi(1, 3)\xi(2, 4)] + \right. \\ &\quad \frac{4}{\lambda} \int \Phi_a(1, 2) \Phi_b(1, 3) [\xi(2, 3) + \xi_3(1, 2, 3)] + \\ &\quad \left. \frac{2}{\lambda^2} \int \Phi_a(1, 2) \Phi_b(1, 2) [1 + \xi(1, 2)] \right\}. \quad (25) \end{aligned}$$

For completeness, we present the result for the three-point correlation function as well

$$\begin{aligned} \langle \delta\tilde{\xi}_3^a \delta\tilde{\xi}_3^b \rangle &= \frac{1}{S^2} \left\{ \int \Phi_a(1, 2, 3) \Phi_b(4, 5, 6) [\xi(1, 2, 3, 4, 5, 6) + \right. \\ &\quad 3\xi(1, 2)\xi(3, 4, 5, 6) + 9\xi(1, 4)\xi(2, 3, 5, 6) + \\ &\quad \left. 3\xi(4, 5)\xi(1, 2, 3, 6) + 9\xi(1, 5, 6)\xi(2, 3, 4) + \right. \end{aligned}$$

$$\begin{aligned}
& 9\xi(1, 4)\xi(2, 3)\xi(5, 6) + 6\xi(1, 4)\xi(2, 5)\xi(3, 6)] \\
& \frac{9}{\lambda} \int \Phi_a(1, 2, 3)\Phi_b(1, 4, 5) [\xi(1, 2, 3, 4, 5) + \\
& \xi(2, 3, 4, 5) + 2\xi(1, 2)\xi(3, 4, 5) + \\
& 2\xi(1, 4)\xi(2, 3, 5) + \xi(2, 3)\xi(1, 4, 5) + \\
& 4\xi(2, 5)\xi(1, 3, 4) + \xi(4, 5)\xi(1, 2, 3) + \\
& \xi(2, 3)\xi(4, 5) + 2\xi(2, 4)\xi(3, 5)] + \\
& \frac{18}{\lambda^2} \int \Phi_a(1, 2, 3)\Phi_b(1, 2, 4) [\xi(1, 2, 3, 4) + \\
& 2\xi(1, 3, 4) + \xi(1, 2)\xi(3, 4) + \\
& 2\xi(1, 3)\xi(2, 4) + \xi(3, 4)] \\
& \left. \frac{6}{\lambda^3} \int \Phi_a(1, 2, 3)\Phi_b(1, 2, 3) [\xi(1, 2, 3) + 3\xi(1, 2) + 1] \right\}. \quad (26)
\end{aligned}$$

In the above formula, ξ with N variables is an N -point correlation function, Φ_a is a bin function corresponding to a triangle (it's value is one, when the triplet is in the bin, 0 otherwise).

The above integral is fairly complicated to calculate in practice, usually some approximations are necessary. In series of papers [18, 5, 7] has worked out practical approximations for up to $N = 4$ for the moments of CIC, obtained (lengthy) semi-analytical formulae, and checked validity of those approximations against simulations. The resulting code (FORtran for Cosmic Errors, FORCE is available publicly.² The errors of CIC have the special property that they contain terms $\propto 1/C$, where C is the number of cells used for the CIC estimation (measurement errors). This is the motivation for algorithms with have $C = \infty$.

From the above error calculations an intuitive physical picture has emerged. We can distinguish three classes of errors, often approximately separated in the final expressions: finite volume errors (the term cosmic variance is used in CMB literature), corresponding to the the fact that the universe might have fluctuations on scales larger than the survey size (the smallness of such fluctuations often termed qualitatively as “representative volume”); discreteness errors: arising from the fact that we are sampling the dark matter distribution (presumably continuous) at finite points with galaxies; edge effect errors, arising from the uneven weights given to galaxies during the estimation. For typical galaxy surveys, edge effects dominate on large scales, and discreteness on small scales. Finite volume effects change slower, and they might dominate in the transition region on intermediate scales. In the above example for the two-point function, the first term contains mainly finite volume effects (the integral of the 4-point function), and terms with powers of $1/\lambda$ are discreteness effects. Edge effects are due to the complicated weight summation blended with the other effects.

²<http://www.ifa.hawaii.edu/users/szapudi/force.html>

These qualitative observations are valid for CMB as well with some caveats: i) the CMB is Gaussian to good approximation, therefore typically only two point functions need to be taken into account ii) the CMB is continuous, i.e. there are no discreteness effects, iii) instead, there are terms arising from the noise of the detection with similar role to discreteness (noise) in LSS. Note that for high precision cosmology applications constraining cosmological parameters, “error on the error” (or uncertainty of the uncertainty as sometimes called) is as important as the size of the error.

5 Symmetry Considerations

A class of functions subject to (Lie-group) symmetries is best represented as an expansion over irreducible representations. In Euclidean (flat) space translation invariance is the most obvious symmetry. The appropriate transform is the Fourier transform, and homogeneity can be taken into account as a Dirac delta function in transform space. The customary definition of the power spectrum and bispectrum are with the Fourier transform of the random fluctuation field $\delta(k)$ as

$$\begin{aligned} \langle \delta(k_1)\delta(k_2) \rangle &= (2\pi)^D \delta_D(k_1 + k_2) P(k_1) \\ \langle \delta(k_1)\delta(k_2)\delta(k_3) \rangle &= (2\pi)^D \delta_D(k_1 + k_2 + k_3) B(k_1, k_2, k_3), \end{aligned} \quad (27)$$

where δ_D is a Dirac delta function, and D is the spatial dimension. Thus, because of homogeneity, the two-point function becomes the Fourier transform of the power spectrum

$$\xi(x_1, x_2) = \int \frac{d^D k}{(2\pi)^D} P(k) e^{ik(x_1 - x_2)}, \quad (28)$$

and a similar equation is true for the three-point correlation function

$$\xi(x_1, x_2, x_3) = \int \prod_{i=1}^3 \frac{d^D k_i}{(2\pi)^D} B(k_1, k_2, k_3) e^{i(k_1 x_1 + k_2 x_2 + k_3 x_3)} \delta_D(k_1 + k_2 + k_3). \quad (29)$$

From these equations, the two-point correlation function is only a function of the difference of its two arguments. If the statistical properties of the underlying field are isotropic as well, these equations can be further simplified. We quote the results for two and three spatial dimensions:

$$\begin{aligned} \xi(r) &= \int \frac{k dk}{2\pi} P(k) J_0(kr) \quad 2\text{D}, \\ \xi(r) &= \int \frac{k^2 dk}{2\pi^2} P(k) j_0(kr) \quad 3\text{D}, \end{aligned} \quad (30)$$

where J_0 and j_0 are ordinary and spherical Bessel functions, respectively.

As a consequence of spherical symmetry the three-point correlation function and the bispectrum, depend only on the shape of a triangle. [19] has

observed that the three-point statistics can be expressed with two unit vectors, thus zero angular momentum bipolar expansion is suitable in 3 spatial dimensions under SO(3) symmetry. Zero angular momentum bipolar functions are proportional to the Legendre polynomials, thus in turn this becomes multi-pole expansion of the bispectrum. If we parameterize the bispectrum as depending on two vectors, and the angle between, this can be written as

$$B(k_1, k_2, \theta) = \sum_l B_l(k_1, k_2) P_l(\cos \theta) \frac{2l+1}{4\pi}, \quad (31)$$

with an entirely similar expansion for the three-point correlation function. It is then simple matter to show [19] that the multi-poles of the bispectrum are related to the multi-poles of the three-point correlation function via a double Hankel transform

$$\xi_l^3(r_1, r_2) = \int \frac{k_1^2}{2\pi^2} dk_1 \frac{k_2^2}{2\pi^2} dk_2 (-1)^l B_l(k_1, k_2) j_l(k_1 r_1) j_l(k_2 r_2). \quad (32)$$

B_l 's and ξ_l are analogous to the C_l 's of the angular power spectrum, they correspond to an angular power spectrum of a shells of three-point statistics.

In two dimensions, the situation is entirely analogous: the symmetry is just U(1) rotations on a ring, thus the correct expansion is Fourier (actually cosine) transform

$$B(k_1, k_2, \theta) = \frac{B_0(k_1, k_2)}{2} + \sum_{n < 0} B_n(k_1, k_2) \cos(n\theta), \quad (33)$$

with analogous expansion for the three-point correlation functions. Note that the sin modes are killed by parity. This expansion is generally applicable for any three-point statistics in isotropic 2-dimensional spaces. This in turn renders the connection of the Fourier coefficients of the three-point correlation function and bispectrum as

$$\xi_n^3(r_1, r_2) = \int \frac{k_1}{2\pi} dk_1 \frac{k_2}{2\pi} dk_2 (-1)^n B_n(k_1, k_2) J_n(k_1 r_1) J_n(k_2 r_2). \quad (34)$$

This latter equation, derived for two-dimensional Euclidean space, is also applicable to the spherical bispectrum in the flat sky approximation. This provides surprisingly accurate results, even for relatively low multi-poles. A form equivalent to the expansion of Eq. 34 was proposed independently by [20] as well, for the (redshift space) projected bispectrum; this is yet another application of the flat sky approximation.

6 Algorithms

Estimation higher order statistics is a daunting computational problem. Naive solutions are typically ranging from the inefficient (for two-point correlations

and counts in cells) to the impossible, hence the application of advanced computer science is a must.

For counts in cells, the naive algorithms scales as MN_C where is preferably $N_C \gtrsim 10^{9-12}$, the number of cells used for the estimation.

Naive estimation estimation of N -point quantities typically scales M^N where M is the number of data points. For modern data sets $M \gtrsim 10^{6-10}$, this becomes prohibitive for higher than second order correlation functions. This is a fast developing field. Next we present a set of algorithms to illustrate the problems and typical solutions.

6.1 N -point Correlation Functions

Hierarchical Algorithms

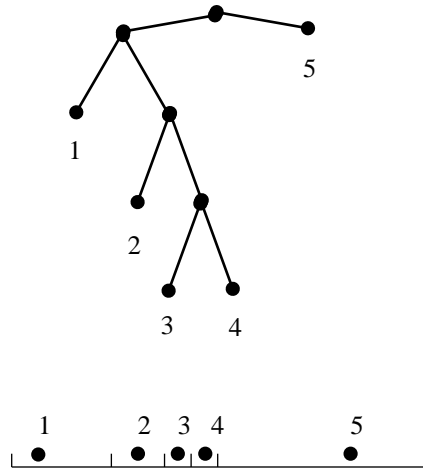


Fig. 1. This figure illustrates a tree data structure of points in 1 dimensions. In this construct, points spatially close, are also stored nearby. Tree structure is similar for continuous field, except there is no early termination of the tree (such as that of number 5 on the figure).

Finding (joint) averages like $\langle \delta_1 \dots \delta_N \rangle$ of a random field δ , where the N -points are taken at a particular configuration, can be done through summation of N -tuples. For the proper averages, the same algorithm is used for the data, and a random set describing the geometry of the survey. For the Monte Carlo estimators an ensemble of mixed N -tuples need to be counted, but again the same algorithm applies without further complexity. The algorithm for $N = 2$ is described next; higher orders are exactly analogous, although more tedious to describe. For details see [21]

The spatial configuration of the two-point function is characterized by the distance r between the two points: this should lie within a bin, i.e. $b_1 < r \leq b_2$. An algorithm capable of calculating the sum $\sum_{r_{12} \leq b} \delta_1 \delta_2$ for any b yields the answer for a proper bin $b_1 < r \leq b_2$ as a difference.

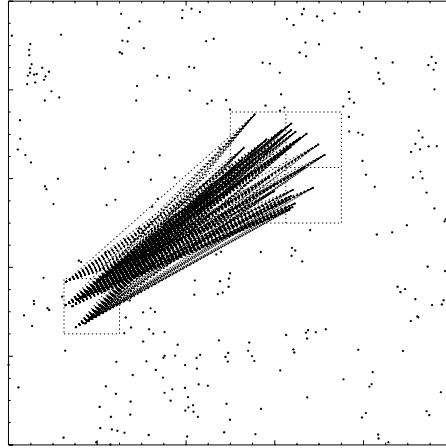


Fig. 2. A particular state of the algorithm is represented. The two squares illustrate two nodes of the tree, which contain the points inside. The number of points is cached, i.e. available at this level of the tree. The pairs of distances between points are marked with lines. If case i) or ii) is true (see text), none of these distances have to be checked, which in turn furnishes the speed-up of the algorithm. The smaller squares within the large square represent the case iii) when the tree has to be split; then the query is run again recursively.

The data points or the pixels of the continuous field can be arranged in a tree data structure. At every level we store the number of elements (or values) below, i.e. sufficient cached statistics. The sum needed then can be calculated by a recursive double search on the tree starting from the root. If the two nodes are n_1 and n_2 with values δ_1 and δ_2 let us denote with r any distance between points of n_1 and n_2 (the lines between the squares of Figure 2. If we can prove that i) for any $r > b \rightarrow$ return, or ii) for any $r \leq b \rightarrow$ add $\delta_1 \times \delta_2$ to the sum and return, (we are done), else iii) split the tree and continue recursively. In worst case this procedure descends to the leaves of the tree, but typically huge savings are realized when whole chunks of data can be taken into account at coarser levels of the tree.

Algorithms Based on Fourier Transforms

As shown next, pair summation can be reformulated to make use of Fast Fourier Transforms, one of fastest algorithms in existence. If $P(x) = a_0 +$

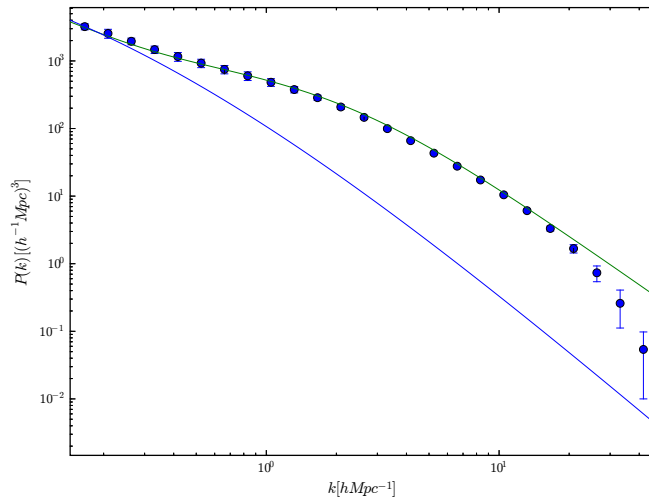


Fig. 3. The power spectrum measured in the VLS (Virgo) simulations. The two-point correlation function have been measured with a fast hierarchical algorithm, and the edge corrected power spectrum was obtained from Eq. 30. The errorbars are calculated from 8 sub-cubes from the simulation, and the two curves show the linear and non-linear theoretical power spectra [22]. The measurement of the correlation function with the Fourier algorithm is even faster, and produces identical results.

$a_1 x + \dots + a_{n-1}$ is a polynomial, and $\epsilon = e^{2\pi i/r}$ unit roots, the coefficients of a discrete Fourier transform of the series a_i can be defined as

$$\hat{a}_k = P(\epsilon^k) = a_0 + a_1 \epsilon^k + \dots + a_{n-1} \epsilon^{(n-1)k}. \quad (35)$$

Direct calculation confirms that $\sum a_k b_{k+\Delta}$ can be calculated by Fourier transforming the series a_i and b_i , multiplying the resulting $\hat{a}_k \hat{b}_k^*$, and finally inverse Fourier transforming back. This simple observation is the discrete analog of the Wiener-Khinchin theorem. To obtain correlation one has to work through subtleties involved with with the periodic boundary conditions, and multidimensionality. The final result is a probably fastest algorithm for calculating correlation functions.

The algorithm in broad terms consists of i) placing the points in a sufficiently fine grid, storing the value $N_{\mathbf{k}}$, the number of objects at (vector) grid point \mathbf{k} , (this step is omitted if the density field is given, such as CMB maps), ii) calculating fluctuations of the field by $\delta = (N - \langle N \rangle) / \langle N \rangle$, iii) discrete Fourier transform with a fast FFT engine, iv) multiplying the coefficients v) Fourier transform back. The same procedure is followed for the mask with zero padding large enough to avoid aliasing effects. The resulting inhomogeneous correlation function is a generalization of the one obtained in

the previous subsections; the usual (homogeneous) correlation function can be obtained by summing over spherical shells. Edge effect corrected power spectrum is obtained with yet another Fourier transform. Measurement of the correlation function on a 768^3 grid takes about 15 minutes on one Opteron processor (cf. Figure ??).

Pure Fourier algorithms are not practical for edge corrected three-point statistics. However, it is possible to combine hierarchical and Fourier methods, to obtain an algorithm which is faster than either of them. In Figure 4I show measurements with such an algorithm in 8 realizations of 260 million particle VLS [51] simulations in a $239.5h^{-1}\text{Mpc}$ cube. The measurement using $\simeq 1400$ bins on a 100^3 grid ($\equiv 10^{15}$ triangles) took less than three hours on a 2.4Ghz single CPU.

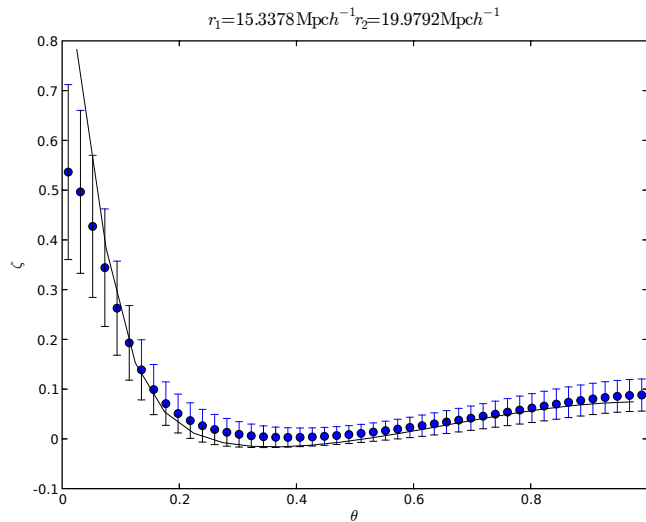


Fig. 4. The three-point correlation function measured with a Fourier based algorithm. The data used is the same as Fig. 3. Theory (solid line) is calculated through Eq. 39. Pure leading order perturbation theory is used, no smoothing effects or non-linearities are taken into account, which probably account for small differences, besides cosmic variance. Note that errorbars, estimated from the same 8 sub-cubes as in the previous figure, are highly correlated.

6.2 Counts in cells algorithms

I present four different algorithms for counts-in-cells, because each of them is optimal for different purposes: algorithm I. calculates counts in cells with infinite sampling for small scales, II. is a massively oversampling algorithm for

large scales, III. is a massively oversampling algorithm for intermediate/small scales, while IV. is a massively oversampling algorithm for large scales and arbitrary cell shapes/sizes. II. and IV. have very similar performance, although II. is more straightforward to generalize for lensing and compensated filters, while IV. has more flexibility in terms of cell shape/size. Together I-IV. covers the full dynamic range of future surveys, with ample overlap between them for cross check.

CIC I: sweep

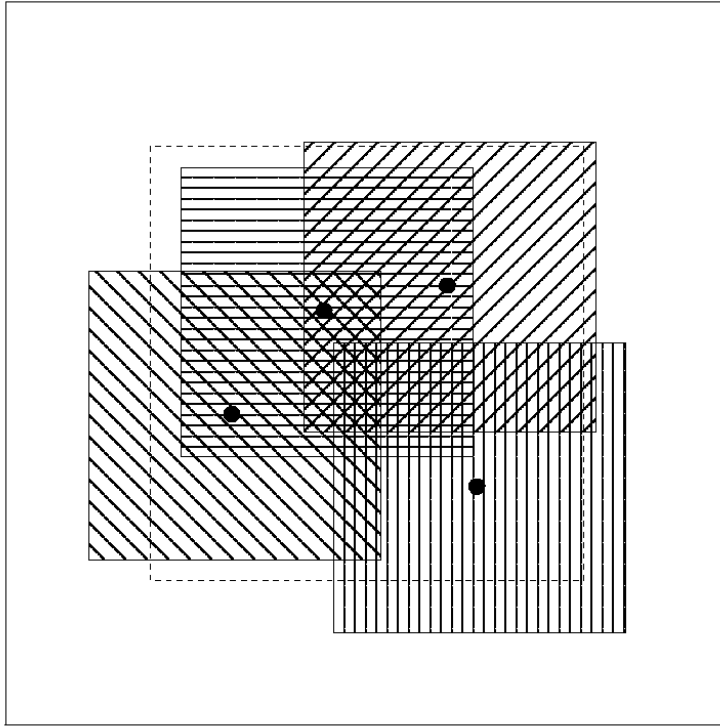


Fig. 5. Illustrates the geometric calculation of counts in cells. There are four points within the solid boundary. The centers of square cells can lie within the dashed boundary. Around each point a square is drawn to represent the possible centers of cells which contain that point. The problem of counts in cells can now be reformulated as calculation of the ratios of all overlap areas (represented with different shadings on the figure) within the dashed boundary.

This algorithm uses the well known “sweep” paradigm from computational geometry, and it realizes the ideal case of $C = \infty$ number of “random” cells thrown. Here we summarize the basic idea in two dimensions only.

The geometric interpretation of the probability of finding N galaxies in a randomly thrown cell is shown on Figure 5. There are four points in a rectangular box. Around each object (large dots) a square is drawn, identical to the sampling cell used for counts in cells. The possible centers of random cells all lie within the dashed line, which follows the boundary of the bounding box. Since the square around each point corresponds to the possible centers of (random) cells containing that same point, the question can be reformulated in the following way: let us partition the area of the possible centers of cells according to the overlap properties of the cells drawn around the objects. The ratio of the area with N overlaps to the total area corresponds to P_N .

Imagine a rigid vertical line moving slowly from the left of Figure 5. towards the right; the boundary can be ignored temporarily. Before the line touches any of the squares, it sweeps through an area contributing to P_0 . Therefore at the point of first contact all the swept area contributes to P_0 and can be recorded. After the contact the line is divided into segments sweeping through areas contributing to P_0 and P_1 respectively. The boundaries of these segments can be imagined as two markers on the line, corresponding to the upper and lower corner the square being touched. As the sweep continues, the results can be recorded at any contact with the side of a square during the movement of the line: the areas swept are assigned according to the markers on the line to different P_N 's. This is done with a one dimensional sweep on the line counting the two kinds of markers. Then the segmentation of the line is updated. Whenever the line makes contact with the left side of a square, two markers are added, whenever it touches the right hand side of a square, the corresponding markers are dropped. The boundaries and rectangular masks, can be trivially taken into account by only starting to record the result of the sweep when entering the area of possible centers. Non-rectangular masks can be converted to rectangular by putting them on a grid.

If there are N objects in the plane, the above procedure will finish after $2N$ updating. The algorithm can be trivially generalized for arbitrary rectangles, any dimensions. For instance in three dimensions the basic sweep is done with a plane, while the plane has to be swept by a line after each contact.

From the definition of the algorithm it follows that the required CPU time scales as $N^D(d/L)^{D(D-1)/2}$ in $D = 2, 3$ dimensions, where N is the number of objects, d/L is the ratio of the scale of the measurement to the characteristic survey length. While for large scales and large D the algorithm becomes impractical, it is clear that for small scales it will be quite fast. It turns out that this is the regime where $C = \infty$ is the most important [18].

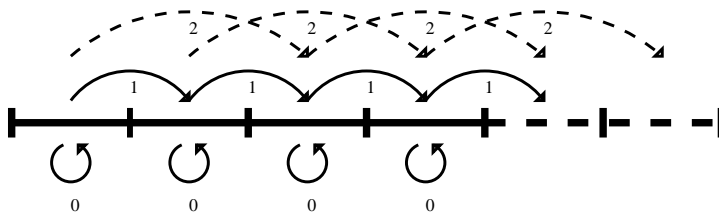


Fig. 6. The successive convolution algorithm is illustrated in one dimension. The solid line represents the grid containing the data, while the dash line corresponds to auxiliary storage repeating the first 2 cells. At the 0th level data is placed in the grid, and counts in cells are calculated. At levels 1 and 2 the solid and dashed arrows respectively represent summations described in the text.

CIC II: successive convolution

This algorithm is essentially a Fourier (or renormalization) style convolution. It will be explained in one dimension for simplicity, generalization is obvious.

The computations are performed on the largest possible grid with N segments which can be fit into the memory of the computer: this determines the smallest possible scale L/N , where L is the box size, and N is the base sampling. A hierarchy of scales are used, with the scale at a given level being twice the scale at one level lower. The results one step lower in the hierarchy are used to keep the number of sampling cells constant even at the largest scales. Counts in cells can be straightforwardly calculated on the resolution scale of the grid, i.e. the smallest scale considered. For the calculation at twice the previous scale the sum of two cells are always stored in one of the cells, for instance in the one with smaller index. Because of the periodic boundary conditions, auxiliary storage is required to calculate the sum of the values in the rightmost cell (if the summations was done left to right), as its right neighbor is the leftmost cell which was overwritten in the first step. After these preparatory steps counts in cells can again be calculated from the N numbers representing partially overlapping cells. For the next level, twice the previous scale, one needs the sum of four original resolution cells: a calculation simply done by summing every other cell of the previous results into one cell. At this level, two auxiliary storage spaces are needed because of the periodicity. In general, at each level in the hierarchy two cells of the previous results are summed as a preparatory step, and counts in cells are calculated simply by computing the frequency distribution of the N sums stored in the main grid. Auxiliary storage is needed for those rightmost cells, which have the periodic neighbors on the left end.

In D dimensions 2^D cells are summed in the preparatory step, and the auxiliary storage space enlarges the original hypercube. The scaling of this algorithm is $C \log C \simeq G \log G$ with a preparation step linear in N .

CIC III: tree

This alternative technique for small scales uses a tree data-structure, similar to the algorithm defined for the N -point correlation functions; it is explained in three dimensions for convenience.

The tree data structure can be thought of as an efficient representation of a sparse array, since at small scales most of the cells are empty in a grid spanning the data. The tree is built up recursively, by always dividing the particles into two groups based on which half of the volume they belong to. The same function is called on both halves with the corresponding particles until there is no particle in the volume, or the scale becomes smaller than a predetermined value. At each level the scale and the number of particles are known, and when an empty volume is reached, all contained volumes are also empty. These two observations are enough to insert the book-keeping needed to calculate counts in cells at all scales while the tree is built. The number of sampling cells at each level are 2^l , where l is the level; the original box is represented by $l = 0$. Towards smaller scales the number of cells increases. When $N^3 = 2^l$, where N is the size of the largest grid of the previous algorithm, the two techniques should (and do) give the exact same answers. At larger scales the previous algorithm is superior, since $N > 2^l$, while this algorithm becomes useful at smaller scales. Just as above, this procedure can be further improved by shifting the particles slightly before calculating the tree. However, since this hierarchy of grids has different numbers of cells, random shifts are more advantageous. Shifting by a fraction of the smallest scale would not exhaust the possibilities for any larger scale, while shifting by a fraction of the largest grid might not shift the underlying grids at all. With the introduction of random shifts (oversampling grids), the dynamic range of algorithms II and III will develop a substantial overlap, which will be useful for testing. This algorithm also scales as $N \log N$ (with preset depth limiting).

CIC IV: cumulative grid

Algorithm II. produces counts in cells results on scales $2^k l$, where l is the scale associated with the base grid. For calculating counts-in-cells distribution for arbitrary scales $[k_1 \times l, k_2 \times l]$, the following construction will be explained in two dimensions; generalization is obvious.

Let us denote the value of the field n_{ij} at the grid-point (i, j) . Let us define another grid, with values $c_{ij} = \sum_{p \leq i, q \leq j} n_{pq}$. Then the number of elements in a cell described by $(i, j), (i + k_1, j + k_2)$ can be calculated simply from $c_{ij} + c_{i+k_1, j+k_2} - c_{i+k_1, j} - c_{i, j+k_2}$ (a well known trick in computational geometry). The preprocessing is proportional to N , and counts in cells for arbitrary rectangle can be calculated is linear with $C \simeq G$.

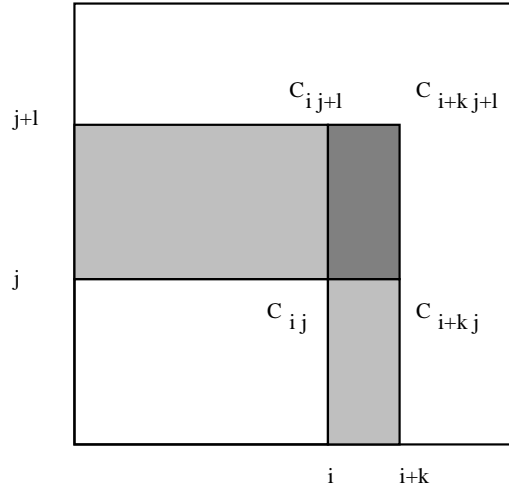


Fig. 7. In the cumulative grid algorithm, each grid point is replaced with a sum of all elements corresponding to rectangles on the figure, with (0,0) as the lower left, and the grid point as the upper right coordinate. The dark shaded area is the required sum, which is calculated as $c_{ij} + c_{i+k_1j+k_2} - c_{i+k_1j} - c_{ij+k_2}$ (see text).

7 Perturbation Theory

On large scales, where the fluctuations are reasonably small, clustering of cosmic structures can be understood in terms of Eulerian weakly non-linear perturbation theory (PT). An excellent exposition is found [2] with substantial reference list. My goal next is to give an extremely cursory, recipe level introduction to the subject.

PT predicts the behavior of any statistics from Gaussian initial conditions, assuming an expansion of the density field into first, second, etc. order, $\delta = \delta^{(1)} + \delta^{(2)} + \dots$. This assumption, when substituted into Euler’s equations for the cosmological dark matter “fluid”, yields a set of consistent equations for the different orders. The resulting perturbative expansion is most conveniently expressed in Fourier space with kernels F_N as,

$$\delta^{(N)}(k) = \int d^3q_1 \dots d^3q_N F_N(q_1, \dots, q_N) \delta_D(q_1 + \dots + q_N - k) \delta^{(1)}(q_1) \dots \delta^{(1)}(q_N) \tag{36}$$

and an analogous equation for the velocity potential. Euler’s equations lead to a simple, albeit “combinatorially exploding” recursion for the kernels [23]. The most important kernel is the first non-trivial F_2

$$F_2(\mathbf{q}_1, \mathbf{q}_2) = 1 + \mu + \left(\frac{q_1}{q_2} + \frac{q_2}{q_1}\right) \cos(\theta) + (1 - \mu) \cos(\theta)^2, \tag{37}$$

where θ is the angle between the two vectors (in this equation explicitly denoted by bold face), and $\mu = \frac{3}{7}\Omega^{-1/140}$ [24].

The leading order calculation of e.g., any third order statistic can be obtained simply by $\langle \delta^3 \rangle_c = \langle (\delta^{(1)} + \delta^{(2)} + \dots)^3 \rangle_c = 3\langle (\delta^{(1)})^2 \delta^{(2)} \rangle + \text{higher orders}$. For Gaussian initial conditions, this leads to formula in terms of $P(k)$, the initial (or linear) power spectrum, and the F_2 kernel.

When the above expansion is executed carefully PT predicts [25, 23, 26, 27] that the bispectrum in the weakly non-linear regime is

$$\left\{ \left(\frac{4}{3} + \frac{2}{3}\mu \right) P_0(x) + \left(\frac{k_1}{k_2} + \frac{k_2}{k_1} \right) P_1(x) + \frac{2}{3}(1 - \mu) P_2(x) \right\} P(k_1)P(k_2) + \text{perm.} \quad (38)$$

where x is the cosine of the angle between the two wave vectors, P_l are Legendre polynomials, and $P(k)$ is the linear power spectrum. We have written the F_2 kernel in terms of Legendre polynomials, to make it explicitly clear that the first permutation depends only on terms up to quadrupole.

Together with the formulae in section 5 this fact can be used for the prediction of the first permutation of three-point correlation function in the weakly nonlinear regime:

$$\begin{aligned} \xi_0^3(r_1, r_2) &= \int \frac{k_1^2}{2\pi^2} dk_1 \frac{k_2^2}{2\pi^2} dk_2 \left(\frac{4}{3} + \frac{2}{3}\mu \right) P(k_1)P(k_2) j_0(k_1 r_1) j_0(k_2 r_2) \\ \xi_1^3(r_1, r_2) &= - \int \frac{k_1^2}{2\pi^2} dk_1 \frac{k_2^2}{2\pi^2} dk_2 \left(\frac{k_1}{k_2} + \frac{k_2}{k_1} \right) P(k_1)P(k_2) j_1(k_1 r_1) j_1(k_2 r_2) \\ \xi_2^3(r_1, r_2) &= \int \frac{k_1^2}{2\pi^2} dk_1 \frac{k_2^2}{2\pi^2} dk_2 \frac{2}{3} (1 - \mu) P(k_1)P(k_2) j_2(k_1 r_1) j_2(k_2 r_2) \end{aligned} \quad (39)$$

I emphasize that the above equation corresponds to the first permutation of the perturbation theory kernel: the other permutations are dealt with the same way, and the results are added. All the integrals factor into one dimensional ones, which simplifies the calculation in practice. It can be shown with tedious calculations that the above formulae are equivalent to [28]. These equations has been used for the predictions of Figure 4. One has to be somewhat careful to integrate the Bessel functions with sufficient accuracy.

For completeness we present the analogous formulae for the projected three-point correlation function (see §9), which is integrated over line of sight coordinates to avoid the effects of redshift distortions. The perturbation theory kernel is simply rewritten in Fourier modes [20]

$$\left\{ \left(\frac{3}{2} - \frac{1}{2}\mu \right) + \left(\frac{k_1}{k_2} + \frac{k_2}{k_1} \right) \cos(\theta) + \frac{1}{2} (1 - \mu) \cos(2\theta) \right\} P(k_1)P(k_2) + \text{perm.} \quad (40)$$

which yields the equivalent result for the projected three-point function ζ^P as

$$\begin{aligned} \zeta_0^P(r_1, r_2) &= \int \frac{k_1}{2\pi} dk_1 \frac{k_2}{2\pi} dk_2 \left(\frac{3}{2} - \frac{1}{2}\mu \right) P(k_1)P(k_2) J_0(k_1 r_1) J_0(k_2 r_2) \\ \zeta_1^P(r_1, r_2) &= - \int \frac{k_1}{2\pi} dk_1 \frac{k_2}{2\pi} dk_2 \left(\frac{k_1}{k_2} + \frac{k_2}{k_1} \right) P(k_1)P(k_2) J_1(k_1 r_1) J_1(k_2 r_2) \\ \zeta_2^P(r_1, r_2) &= \int \frac{k_1}{2\pi} dk_1 \frac{k_2}{2\pi} dk_2 \frac{1}{2} (1 - \mu) P(k_1)P(k_2) J_2(k_1 r_1) J_2(k_2 r_2) \end{aligned} \quad (41)$$

Here both r_i and k_i are two-dimensional vectors perpendicular to the line of sight, and the other two permutations have to be added up as previously.

8 Bias

Most observations record the distribution of “light” at some wavelength (except some still singular cases, such as neutrino astronomy, or air shower detectors), might have spatial distribution different from that of the underlying dark matter or “mass”. This difference means that our estimators might give us a “biased” view of the statistics of the underlying dark matter. This bias is caused by the complex interplay of non-linear gravitational dynamics with dissipative physics. While there have already been advances in ab initio modeling of this complicated process, the most fruitful approach is still phenomenological.

Since galaxy formation is a stochastic process, we can imagine that there is no one-to-one correspondence between dark matter and galaxy density, the former only determines the probability of forming a galaxy (together with its environment and merger history). This general case is called *stochastic* biasing [29, 30], while, if there is a functional dependence between the two fields, it is *deterministic*. In mock catalogs created using semi-analytic galaxy formation models e.g., [31], most of the stochasticity of the bias is simply due to shot noise [32].

If there is a functional relationship between the dark matter and galaxy density fields, the simplest possible relation is *linear*, the more general ones are *non-linear*.

Linear bias is described by the equation of $\delta_g = b\delta_{DM}$, where b is a constant. Note that this is an inconsistent equation for $b > 1$ yielding the minimum value of the galaxy density field $-b < -1$, obviously non-sense. Yet, owing to its simplicity, this is the single most used bias model.

A non-linear generalization contains an arbitrary function $\delta_g = f(\delta_{DM})$. This function can either be assumed to be a general function with a few parameters (e.g. exponential), or can be expanded. The two most used expansions are Taylor expansion, or expansion into Hermite-polynomials (and thereby expanding around a Gaussian).

In the weakly non-linear regime, the coefficients of the Taylor expansion are the non-linear bias coefficients;

$$\delta_g = f(\delta_{DM}) = \sum_N \frac{b_N}{N!} \delta_{DM}^N. \quad (42)$$

This equation can be used perturbatively to calculate the moments of the biased (galaxy) density field in terms of the moments of the underlying field, and bias coefficients [33, 34, 35]. In typical applications, the functional relationship is set up between smoothed fields: it is important to note that

smoothing and biasing are two operations which do not commute. Therefore the bias coefficients have a somewhat obscure physical meaning, as they depend not only on the physics of galaxy formation, but on the nature of smoothing itself. Note also, that the zeroth coefficient b_0 is set to ensure $\langle \delta_g \rangle = 0$, i.e. it is non-zero.

Symmetries can be used to construct estimators which constrain the bias in the weakly non-linear regime. To second order, the biased reduced bispectrum transforms as $q = Q/b + b_2/b^2$ [36], where the lower case denotes the galaxy (measured), and the upper case the dark matter (theory) values. It is clear that b_2 can only effect the monopole term. Thus a simple estimator for the bias can be constructed as [19]

$$\begin{aligned} b &= \frac{Q_1}{q_1} = \frac{Q_2}{q_2} \\ b_2 &= q_0 b^2 - Q_0 b. \end{aligned} \quad (43)$$

According to the equations, the quadrupole to dipole ratio does not depend on the bias, thus it serves as a novel, useful test of the underlying assumptions: a quasi-local perturbative, deterministic bias model and perturbation theory. Figure 4. shows the dipole to quadrupole ratio for BBKS, and EH power spectra, respectively. The range of k 's to be used for bias extraction can be determined from contrasting the measurements with these predictions. Note that scales where baryon oscillations are prominent are barely accessible with present redshift surveys. On smaller scales non-linear evolution is likely to modify these prediction based purely on leading order perturbation theory ([37]).

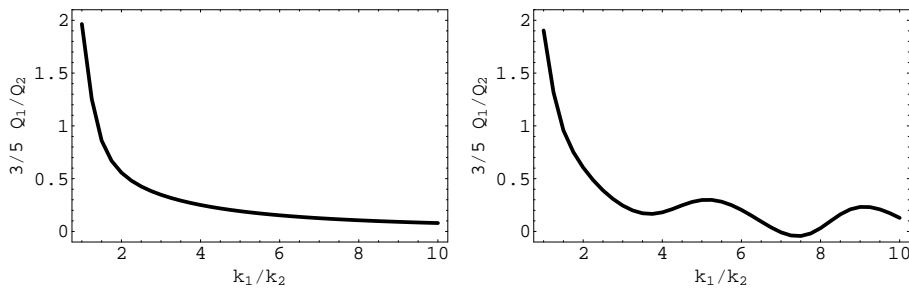


Fig. 8. Left: the dipole to quadrupole ratio $3/5 Q_1/Q_2$ is plotted for a BBKS theory (thick solid line) for $k = 0.01$. The right panel shows the same using the EH fit for comparison, featuring baryonic oscillations.

The above simple theory illustrates that three-point statistics can constrain the first two bias parameters in the weakly non-linear regime. Similarly four point statistics constrain the first three parameters, etc.

An alternative to the above simple theory, and possibly more useful on smaller scales, is the halo model. The physical picture is simple [38]: we try

to model the distribution by some entities, “halos”, which have a relatively simple distribution (from perturbation theory). Large scale correlations thus follow from the “halo-halo” type terms, while all the small scale statistics follows from the halo profile (“1-halo term”), and the distribution of halo masses. In these notes we cannot give justice to halo models, the interested reader is referred to [6], and references therein. Halo models have considerable success in describing the two-point statistics of the dark matter distributions, and they provide a reasonable approximation (currently at the 20% level) to the three-point statistics. Galaxy bias is then described by the halo occupation probabilities.

For halo model predictions, higher order Bessel integrals are needed [39], but the principle is the exactly the same as Eq. 39 (see also [40] for a different approach). While halo models are physically motivated, the best fit parameters differ for two and three-point statistics thus the physical meaning of the parameters is still somewhat nebulous.

9 Redshift Distortions

Redshift distortions, together with biasing, represent the most uncertain aspect of the phenomenology of higher order statistics. Here I only offer a superficial overview of this complicated topic; for a comprehensive review of redshift distortions on two-point statistics, see [41]

The physical idea is fairly simple: in redshift surveys, the radial distance to an object is deduced from its redshift using the Hubble relation in our expanding universe. Therefore, the “peculiar velocity”, the velocity of an object with respect to the average Hubble flow, will add to the measured distance. Such a space, where position of an object is given in a spherical coordinate system with two angles, and a radial distance which contains (a random) velocity is called *redshift space*, as opposed to real space (the one we would really want to measure).

The spatial distribution of objects will no longer be translation invariant, although it will still have rotational symmetry around the observer. The deviation from translation invariance is of the observed distribution is called “redshift distortion”. Qualitatively, it is mainly due to two distinct effects: on small scales, velocity dispersion of virialized clumps will look elongated along the line of sight: popularly called the “finger of god” effect. On larger scales, infall velocities cause distortions perpendicularly to the line of sight, the Kaiser-effect.

The breaking of translational symmetry means that the redshift-space quantities depend on larger number of parameters, e.g. the two- and three-point correlation functions will depend on 3 and 6 parameters respectively (2, and 5 in the distant observer approximation).

Redshift distortions can be taken into account in perturbation theory. In the distant observer approximation, when all lines of sights can be take to be

parallel, the effect has been calculated for the three-point function by [42]. The general case needs a complex multipolar expansions; the results are fairly tedious and will be presented elsewhere.

Besides predicting the redshift space quantities using theory or simulation, one can sweep redshift distortions under the rug by introducing the “projected” correlation functions. These assume a distant observer approximation, where one can consider the N -vectors to pointing from the observer to N vertices of an N -point configuration parallel. Then, one can introduce $\pi - \sigma$ coordinates [3], with π_i vectors parallel to the line of sight, while the σ_i vectors perpendicular to it.

The important point about this parametrization is that, approximately, only π coordinates are affected by redshift distortions. A convenient, redshift distortion free quantity is obtained by integrating over the redshift direction, i.e. π coordinates. The resulting object, the “projected N -point correlation function”, integrated over $N - 1$ π coordinates is free of redshift distortions. Although it is similar to angular (projected) correlation function, the units of the σ coordinates are still $h^{-1}\text{Mpc}$, and, if properly done, its signal to noise is higher.

Fourier space analogs of the above idea use k_{\perp} and k_{\parallel} for perpendicular and parallel k vectors. E.g., the redshift space bispectrum is parametrized by the five parameters $B(k_{1,\perp}, k_{2,\perp}, k_{3,\perp}, k_{1,\parallel}, k_{2,\parallel})$, with \perp denoting transverse, and \parallel parallel quantities with respect to the line of sight in the distant observer approximation. Interestingly, the real space bispectrum can be estimated from taking $k_{1,\parallel} \simeq k_{2,\parallel} \simeq 0$ [19].

10 Example: Conditional Cumulants

In my lectures, I presented an detailed example using a new set of statistics, conditional cumulants, closely following [43]. It illustrates most of the generic features of the theory, baring its strengths and weaknesses.

Conditional cumulants represent an interesting and sensible compromise between N -point correlation functions and cumulants measured from moments of counts in cells. As we will see next, they can be understood as degenerate N -point correlation functions, or integrated monopole moments of the bispectrum, and they are closely related to neighbor counts. They share accurate edge corrected estimators with N -point correlation functions, yet, they are as straightforward to measure and interpret as counts in cells.

10.1 Basics

The general conditional cumulants, Eq. 6, have been defined as the joint connected moment of one unsmoothed and $N - 1$ smoothed density fluctuation fields. In the most general case, each top hat window might have a different

radius. Further simplification arises if all the top hats are the same, i.e. we define $U_N(r)$ with $r_1 = \dots = r_{N-1} = r$ as the degenerate conditional cumulant c.f. [44]. U_N subtly differs from the usual cumulant of smoothed field $\bar{\xi}_N$ by one less integral over the window function.

The second order, U_2 , is equivalent to the (confusingly named) J_3 integral e.g., [3],

$$U_2(r) = \frac{3}{r^3} J_3(r) = \frac{1}{(2\pi)^3} \int P(k) w(kr) 4\pi k^2 dk , \quad (44)$$

where $w(kr) = 3(\sin kr - kr \cos kr)/(kr)^3$ is the Fourier transform of $W_r(s)$, and $P(k)$ is the power spectrum.

For higher orders, we can construct reduced conditional cumulants as

$$R_N(r) = \frac{U_N(r)}{U_2^{N-1}(r)} . \quad (45)$$

Both U_N and R_N have deep connection with moments of neighbor counts e.g., [3] as we show next. Let us define the partition function $Z[J] = \langle \exp(\int iJ\rho) \rangle$ c.f., [4], where ρ is the smooth density field. Then we can use the special source function $iJ(x) = W(x)s + \delta_D(x)t$ to obtain the generating function $G(s, t)$. This is related to the generating function of neighbor counts factorial moments as $G(s) = \partial_t G(s, t)|_{t=0}$. Explicitly,

$$G(s) = \sum_{M \geq 0} \frac{(snv)^M}{M!} U_{M+1} \exp \sum_{N \geq 1} \frac{(snv)^N}{N!} \bar{\xi}_N , \quad (46)$$

where $nv = \bar{N}$ is the average count of galaxies, and $\bar{\xi} = U_1 = 1$ by definition. This generating function can be used to obtain U_N 's and/or R_N 's from neighbor count factorial moments analogously as the generating functions in [45] for obtaining S_N 's from factorial moments of counts in cells. For completeness, the generating function for neighbor counts' distribution is obtained by substituting $s \rightarrow s - 1$, while the ordinary moment generating function by $s \rightarrow e^s - 1$. Expanding $G(e^s - 1)$ recovers the formulae in [3], §36. The above generating function allows the extraction of U_N from neighbor count statistics for high N . The situation is analogous to the CIC theory presented in [45], and it is fully applicable to neighbor counts statistics with minor and trivial modifications.

So far our discussion has been entirely general; in what follows we will focus on $N = 3$, i.e. the first non-trivial conditional cumulant U_3 . $U_3(r_1, r_2)$ is directly related to bispectrum by

$$U_3(r_1, r_2) = \frac{1}{(2\pi)^6} \int B(\mathbf{k}_1, \mathbf{k}_2, \mathbf{k}_3) \delta_D(\mathbf{k}_1 + \mathbf{k}_2 + \mathbf{k}_3) w(k_1 r_1) w(k_2 r_2) d^3 k_1 d^3 k_2 d^3 k_3 , \quad (47)$$

where δ_D is the Dirac delta function. To further elucidate this formula, we use the multipole expansion of bispectrum and three point correlation function of Eqs. 31 and 32 to find

$$U_3(r_1, r_2) = \frac{4\pi}{V_1 V_2} \int_0^{r_1} \int_0^{r_2} \zeta_0(r_1, r_2) r_1^2 r_2^2 dr_1 dr_2 \quad (48)$$

$$= \frac{4\pi}{(2\pi)^6} \int dk_1 dk_2 \frac{3k_1}{r_1} \frac{3k_2}{r_2} j_1(k_1 r_1) j_1(k_2 r_2) B_0(k_1, k_2), \quad (49)$$

in which j_1 is the first order spherical Bessel function. We see the U_3 depends only on the monopole moment of the bispectrum/three-point correlation function. This property significantly simplifies the transformation of this statistic under redshift distortions.

10.2 U_3 in the Weakly Non-linear Perturbation Regime

Using the general machinery of perturbation theory, one can predict the conditional cumulants to leading order as matter of simple calculation. For third order, the results, as usual, will depend on the F_2 kernel, and the linear power spectrum (or correlation function). We leave as an exercise for the reader to show that

$$\begin{aligned} R_3(r_1, r_2) &\equiv \frac{U_3(r_1, r_2)}{U_2(r_1)U_2(r_2)} = \frac{34}{21} \left[1 + \frac{\bar{\xi}(r_1, r_2)}{U_2(r_1)} + \frac{\bar{\xi}(r_1, r_2)}{U_2(r_2)} \right] \\ &+ \frac{1}{3} \frac{\bar{\xi}(r_1, r_2)}{U_2(r_1)} \left[\frac{d \ln U_2(r_2)}{d \ln r_2} + \frac{\partial \ln \bar{\xi}(r_1, r_2)}{\partial \ln r_2} \right] \\ &+ \frac{1}{3} \frac{\bar{\xi}(r_1, r_2)}{U_2(r_2)} \left[\frac{d \ln U_2(r_1)}{d \ln r_1} + \frac{\partial \ln \bar{\xi}(r_1, r_2)}{\partial \ln r_1} \right], \end{aligned} \quad (50)$$

in which $\bar{\xi}(r_1, r_2) = \frac{1}{2\pi^2} \int k^2 P(k) W(kr_1) W(kr_2) dk$. The special case when $r_1 = r_2 = r$ reads

$$R_3 = \frac{34}{21} \left[1 + 2 \frac{\sigma^2}{U_2} \right] + \frac{1}{3} \frac{\sigma^2}{U_2} \left[2 \frac{d \ln U_2}{d \ln r} + \frac{d \ln \sigma^2}{d \ln r} \right], \quad (51)$$

where $\sigma^2 = \frac{1}{2\pi^2} \int k^2 P(k) W^2(kr) dk$. Note the similarity of R_3 with the skewness, which is calculated in weakly non-linear perturbation theory as $S_3 = 34/7 - d \ln \sigma^2 / d \ln r$ [46, 47].

10.3 Measurements of Conditional Cumulants in Simulations

$U_n(r)$ can be measured similarly to N -point correlation functions. For instance U_2 can be thought of as a two point correlation function in a bin $[r_{lo}, r_{hi}] \equiv [0, r]$. Taking the lower limit to be a small number instead of 0, one can avoid discreteness effects due to self counting (this is equivalent to using factorial moments when neighbor counts are calculated directly). Given a set of data and random points, the class of estimators of 17 provides an edge (and incompleteness) corrected technique to measure conditional cumulants. Existing N -point correlation function codes can be used for the estimation; for higher than third order, one also has to take connected moments in the usual way.

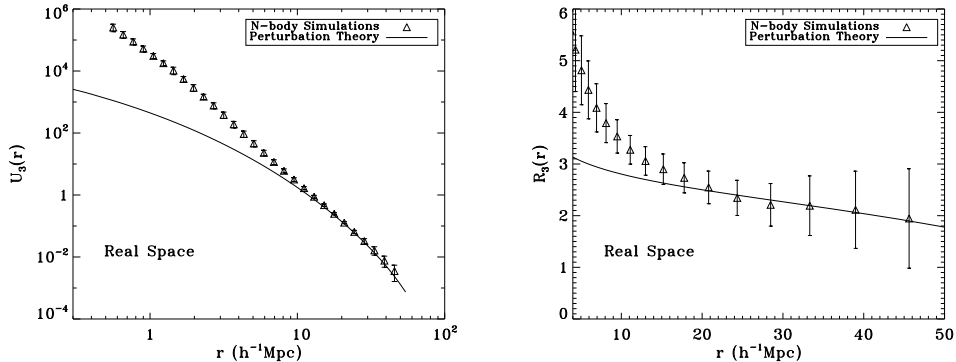


Fig. 9. Predictions of weakly non-linear perturbation theory for third order conditional cumulant U_3 (left), and the reduced statistics R_3 (right) are in real space (solid line) are compared with measurements in N-body simulations (triangles with errorbars) with Λ CDM cosmology. The agreement is remarkable above $\gtrsim 20h^{-1}\text{Mpc}$

While the above suggests a scaling similar to N -point correlation functions, the relation to neighbor count factorial moments outlined in the previous section can be used to realize the estimator using two-point correlation function codes. To develop such an estimator, neighbor count factorial moments need to be collected for each possible combinations, where data and random points play the role of center and neighbor.

Note that the edge correction of Eq. (17) is expected to be less accurate for conditional cumulants, than for N -point correlation functions, however, the estimator will be more accurate than CIC estimators. Several alternative ways for correcting edge effects are known, which would be directly applicable to conditional cumulants [48, 49, 50]. In what follows, we use Eq. (17) for all results presented.

To test PT of the conditional cumulants, we performed measurements in Λ CDM simulations by the Virgo Supercomputing Consortium [51]. We used outputs of the Virgo simulation and the VLS (Very Large Simulation). Except for box sizes and number of particles, these two simulations have identical cosmology parameters: $\Omega_m = 0.3$, $\Omega_v = 0.7$, $\Gamma = 0.21$, $h = 0.7$ and $\sigma_8 = 0.9$. In order to estimate measurement errors, we divide the VLS simulation into eight independent subsets each with the same size and geometry the original Virgo simulation. In total, we have used the resulting nine realizations to estimate errors. Note that we corrected for cosmic bias by always taking the average before ratio statistics were formed.

Our measurements of the second and third order conditional cumulants are displayed in Figs. 1 and 2, respectively. Results from EPT (Eq. 51) are denoted with solid lines. The measurements in simulations are in excellent agreement with EPT, especially on large scales $\gtrsim 20h^{-1}\text{Mpc}$.

10.4 Redshift Distortions

As three-dimensional galaxy catalogs are produced inherently in redshift space, understanding effects of redshift distortions on these statistics is crucial before practical applications can follow. In the distant observer approximation, the formula by [52, 53] is expected to provide an excellent approximation for $U_2(r)$. According to §2, we only need to consider the monopole enhancement

$$U_2(s) = \left(1 + \frac{2}{3}f + \frac{1}{5}f^2\right) U_2(r) , \quad (52)$$

where $f \approx \Omega_m^{0.6}$. This formula essentially predicts a uniform shift of the real space results. To test it, we repeated our measurements in redshift space, and found that the above is indeed an excellent approximation in redshift space.

Considering the relatively simple, monopole nature of the statistics, we expect that the overall effect on U_3 should also be a simple shift, similarly to the Lagrangian calculations by [27] and the more general Eulerian results by [42]. Specifically, we propose that ratio of R_3 in redshift space to that in real space can be approximated by

$$\frac{5(2520 + 3360f + 1260f^2 + 9f^3 - 14f^4)}{98(15 + 10f + 3f^2)^2} \cdot \frac{7}{4} . \quad (53)$$

This is motivated by the notion that the shift from redshift distortions of equilateral triangles should be similar to the corresponding shift for our monopole statistic. Our simulation results (see Fig. 3) show that this simple idea is indeed a surprisingly good approximation, although the phenomenological theory based on the above formula appears to have $\simeq 5\%$ bias on scales $\gtrsim 20h^{-1}\text{Mpc}$ where we expect that weakly non-linear perturbation theory is a good approximation. For practical applications, this bias can be calibrated by N -body, or 2LPT [54] simulations.

In addition to the above simple formula, we have calculated the shift due to redshift distortions by angular averaging the bispectrum monopole term in [42]. We have found that the results over-predict redshift distortions, however, they would agree with simulations at the 1-2% level if we halved the terms classified as FOG (finger of god). At the moment there is no justification for such a fudge factor, therefore we opt to use the above phenomenology, which is about 5% accurate. While redshift distortions of third order statistics are still not fully understood due to the non-perturbative nature of the redshift space mapping (R. Scoccimarro, private communication), detailed calculations taking into account velocity dispersion effects will improve the accuracy of the redshift space theory U_3 .

For applications to constrain bias, one has to keep in mind that redshift distortions and non-linear bias do not commute. However, at the level of the above simple theory, it is clear that one can understand the important effects at least for the third order statistic. There are several ways to apply

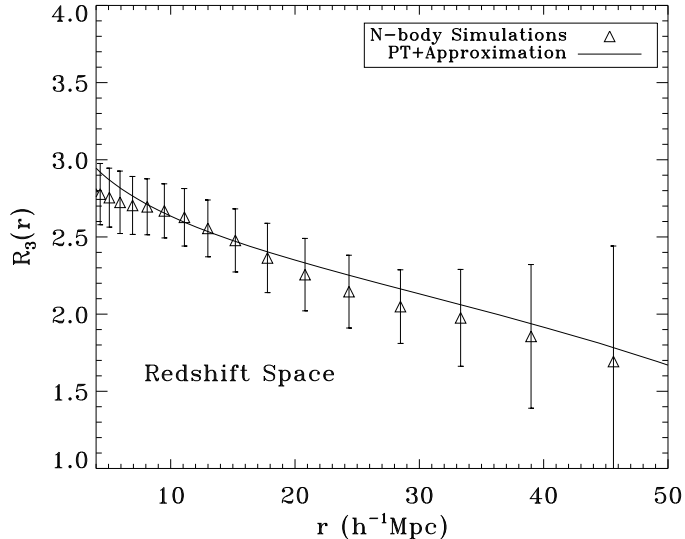


Fig. 10. Same as Figure 2, lower panel, but for R_3 in redshift space. The solid line shows phenomenological model based on Equation 53. The theory appears to be a reasonable approximation at the 5% level.

conditional cumulants for bias determination, either via combination with another statistic [55], or using the configuration dependence of the more general $R_3(r_1, r_2)$. One also has to be careful that in practical applications ratio statistics will contain cosmic bias [56]. We propose that joint estimation with U_2 and U_3 will be more fruitful, even if R_3 is better for plotting purposes. Details of the techniques to constrain bias from these statistics, as well as determination of the bias from wide field redshift surveys is left for future work.

Another way to get around redshift distortions is to adapt conditional cumulants for projected and angular quantities. Such calculations are straightforward, and entirely analogous to those performed for S_3 in the past. Further possible generalization of our theory would be to use halo models [6] to extend the range of applicability of the theory well below $20h^{-1}\text{Mpc}$. These generalizations are left for subsequent research.

11 Acknowledgments

This work was supported by NASA through grants AISR NAG5-11996, ATP NAG5-12101, and by NSF through grants AST02-06243 and ITR 1120201-128440, as well as Valencia summer school, one of the best organized and

most enjoyable ever. The author would like to thank Stephane Colombi, Pablo Fosalba, Jun Pan, Simon Prunet, Alex Szalay for many discussions and contributions. The simulations used have been carried out by the Virgo Supercomputing Consortium using computers based at Computing Centre of the Max-Planck Society in Garching and at the Edinburgh Parallel Computing Centre³.

References

1. V. J. Martinez and E. Saar, *Statistics of the Galaxy Distribution*, Chapman and Hall/CRC Press, Boca Raton, USA, 2002.
2. F. Bernardeau, S. Colombi, E. Gaztanaga, and R. Scoccimarro, “Large-scale structure of the Universe and cosmological perturbation theory,” *Phys. Rep.* **367**, pp. 1–128, 2002.
3. P. J. E. Peebles, *The large-scale structure of the universe*, Research supported by the National Science Foundation. Princeton, N.J., Princeton University Press, 1980. 435 p., 1980.
4. I. Szapudi and A. S. Szalay, “Higher order statistics of the galaxy distribution using generating functions,” *ApJ* **408**, pp. 43–56, May 1993.
5. I. Szapudi, S. Colombi, A. Jenkins, and J. Colberg, “Experimental cosmic statistics - II. Distribution,” *MNRAS* **313**, pp. 725–733, Apr. 2000.
6. A. Cooray and R. Sheth, “Halo models of large scale structure,” *Phys. Rep.* **372**, pp. 1–129, Dec. 2002.
7. I. Szapudi, M. Postman, T. R. Lauer, and W. Oegerle, “Observational Constraints on Higher Order Clustering up to $z \sim 1$,” *ApJ* **548**, pp. 114–126, Feb. 2001.
8. H. A. Feldman, N. Kaiser, and J. A. Peacock, “Power-spectrum analysis of three-dimensional redshift surveys,” *ApJ* **426**, pp. 23–37, May 1994.
9. S. D. Landy and A. S. Szalay, “Bias and variance of angular correlation functions,” *ApJ* **412**, pp. 64–71, July 1993.
10. S. Szapudi and A. S. Szalay, “A New Class of Estimators for the N-Point Correlations,” *ApJ* **494**, pp. L41+, Feb. 1998.
11. I. Szapudi and A. S. Szalay, “The Variance in a New Class of N-point Estimators in Poisson and Binomial Point Processes,” *Annales de l’I.S.U.P.*, p. I, 2000.
12. J. R. Bond, A. H. Jaffe, and L. Knox, “Estimating the power spectrum of the cosmic microwave background,” *Phys. Rev. D* **57**, pp. 2117–2137, Feb. 1998.
13. M. Tegmark, A. J. S. Hamilton, M. A. Strauss, M. S. Vogeley, and A. S. Szalay, “Measuring the Galaxy Power Spectrum with Future Redshift Surveys,” *ApJ* **499**, pp. 555–+, May 1998.
14. S. P. Oh, D. N. Spergel, and G. Hinshaw, “An Efficient Technique to Determine the Power Spectrum from Cosmic Microwave Background Sky Maps,” *ApJ* **510**, pp. 551–563, Jan. 1999.
15. A. J. S. Hamilton, “Uncorrelated modes of the non-linear power spectrum,” *MNRAS* **312**, pp. 257–284, Feb. 2000.

³The data are publicly available at <http://www.mpa-garching.mpg.de/Virgo>

16. M. G. Santos, A. Heavens, A. Balbi, J. Borrill, P. G. Ferreira, S. Hanany, A. H. Jaffe, A. T. Lee, B. Rabii, P. L. Richards, G. F. Smoot, R. Stompor, C. D. Winant, and J. H. P. Wu, "Multiple methods for estimating the bispectrum of the cosmic microwave background with application to the MAXIMA data," *MNRAS* **341**, pp. 623–643, May 2003.
17. A. Heavens, M. Santos, and P. Ferreira, "The bispectrum of MAXIMA," *New Astronomy Review* **47**, pp. 815–820, Nov. 2003.
18. I. Szapudi and S. Colombi, "Cosmic Error and Statistics of Large-Scale Structure," *ApJ* **470**, pp. 131–+, Oct. 1996.
19. I. Szapudi, "Three-Point Statistics from a New Perspective," *ApJ* **605**, pp. L89–L92, Apr. 2004.
20. Z. Zheng, "Projected Three-Point Correlation Functions and Galaxy Bias," *ApJ* **614**, pp. 527–532, Oct. 2004.
21. A. W. Moore, A. J. Connolly, C. Genovese, A. Gray, L. Grone, N. Kanidoris, R. C. Nichol, J. Schneider, A. S. Szalay, I. Szapudi, and L. Wasserman, "Fast Algorithms and Efficient Statistics: N-Point Correlation Functions," in *Mining the Sky*, pp. 71–+, 2001.
22. R. E. Smith, J. A. Peacock, A. Jenkins, S. D. M. White, C. S. Frenk, F. R. Pearce, P. A. Thomas, G. Efstathiou, and H. M. P. Couchman, "Stable clustering, the halo model and non-linear cosmological power spectra," *MNRAS* **341**, pp. 1311–1332, June 2003.
23. M. H. Goroff, B. Grinstein, S.-J. Rey, and M. B. Wise, "Coupling of modes of cosmological mass density fluctuations," *ApJ* **311**, pp. 6–14, Dec. 1986.
24. M. Kamionkowski and A. Buchalter, "Weakly Nonlinear Clustering for Arbitrary Expansion Histories," *ApJ* **514**, pp. 7–11, Mar. 1999.
25. J. N. Fry, "The Galaxy correlation hierarchy in perturbation theory," *ApJ* **279**, pp. 499–510, Apr. 1984.
26. F. R. Bouchet, S. Colombi, E. Hivon, and R. Juszkiewicz, "Perturbative Lagrangian approach to gravitational instability," *A&A* **296**, pp. 575–+, Apr. 1995.
27. E. Hivon, F. R. Bouchet, S. Colombi, and R. Juszkiewicz, "Redshift distortions of clustering: a Lagrangian approach," *A&A* **298**, pp. 643–+, June 1995.
28. Y. P. Jing and G. Boerner, "Three-point correlation function in the quasilinear regime," *A&A* **318**, pp. 667–672, Feb. 1997.
29. A. Dekel and O. Lahav, "Stochastic Nonlinear Galaxy Biasing," *ApJ* **520**, pp. 24–34, July 1999.
30. R. J. Scherrer and D. H. Weinberg, "Constraints on the Effects of Locally Biased Galaxy Formation," *ApJ* **504**, pp. 607–+, Sept. 1998.
31. A. J. Benson, S. Cole, C. S. Frenk, C. M. Baugh, and C. G. Lacey, "The nature of galaxy bias and clustering," *MNRAS* **311**, pp. 793–808, Feb. 2000.
32. I. Szapudi and J. Pan, "On Recovering the Nonlinear Bias Function from Counts-in-Cells Measurements," *ApJ* **602**, pp. 26–37, Feb. 2004.
33. I. Szapudi, *Higher order correlations*, Master's Thesis, Eotvos University, Budapest, 1990.
34. J. N. Fry and E. Gaztanaga, "Biasing and hierarchical statistics in large-scale structure," *ApJ* **413**, pp. 447–452, Aug. 1993.
35. T. Matsubara, "Diagrammatic Methods in Statistics and Biasing in the Large-Scale Structure of the Universe," *ApJS* **101**, pp. 1–+, Nov. 1995.
36. J. N. Fry, "The minimal power spectrum: Higher order contributions," *ApJ* **421**, pp. 21–26, Jan. 1994.

37. A. Meiksin, M. White, and J. A. Peacock, “Baryonic signatures in large-scale structure,” *MNRAS* **304**, pp. 851–864, Apr. 1999.
38. R. M. Soneira and P. J. E. Peebles, “Is there evidence for a spatially homogeneous population of field galaxies,” *ApJ* **211**, pp. 1–15, Jan. 1977.
39. P. Fosalba, J. Pan, and I. Szapudi, “Cosmological Three-Point Function: Testing The Halo Model Against Simulations,” *ArXiv Astrophysics e-prints*, 2005.
40. M. Takada and B. Jain, “The three-point correlation function in cosmology,” *MNRAS* **340**, pp. 580–608, Apr. 2003.
41. A. J. S. Hamilton, “Linear Redshift Distortions: a Review,” in *ASSL Vol. 231: The Evolving Universe*, pp. 185–+, 1998.
42. R. Scoccimarro, H. M. P. Couchman, and J. A. Frieman, “The Bispectrum as a Signature of Gravitational Instability in Redshift Space,” *ApJ* **517**, pp. 531–540, June 1999.
43. J. Pan and I. Szapudi, “Conditional Cumulants in Weakly Non-linear Regime,” *ArXiv Astrophysics e-prints*, May 2004.
44. S. A. Bonometto, S. Borgani, S. Ghigna, A. Klypin, and J. R. Primack, “Non-linear clustering in the cold plus hot dark matter model,” *MNRAS* **273**, pp. 101–121, Mar. 1995.
45. I. Szapudi and A. S. Szalay, “Higher order statistics of the galaxy distribution using generating functions,” *ApJ* **408**, pp. 43–56, May 1993.
46. R. Juszkiewicz, F. R. Bouchet, and S. Colombi, “Skewness induced by gravity,” *ApJ* **412**, pp. L9–L12, July 1993.
47. F. Bernardeau, “The effects of smoothing on the statistical properties of large-scale cosmic fields,” *A&A* **291**, pp. 697–712, Nov. 1994.
48. B. Ripley, *Statistical inference for spatial processes*, University Press, Cambridge, 1988.
49. M. Kerscher, I. Szapudi, and A. S. Szalay, “A Comparison of Estimators for the Two-Point Correlation Function,” *ApJ* **535**, pp. L13–L16, May 2000.
50. J. Pan and P. Coles, “Boundary corrections in fractal analysis of galaxy surveys,” *MNRAS* **330**, pp. 719–730, Mar. 2002.
51. A. Jenkins, C. S. Frenk, F. R. Pearce, P. A. Thomas, J. M. Colberg, S. D. M. White, H. M. P. Couchman, J. A. Peacock, G. Efstathiou, and A. H. Nelson, “Evolution of Structure in Cold Dark Matter Universes,” *ApJ* **499**, pp. 20–+, May 1998.
52. N. Kaiser, “Clustering in real space and in redshift space,” *MNRAS* **227**, pp. 1–21, July 1987.
53. P. B. Lilje and G. Efstathiou, “Gravitationally induced velocity fields in the universe. I - Correlation functions,” *MNRAS* **236**, pp. 851–864, Feb. 1989.
54. R. Scoccimarro, “Gravitational Clustering from χ^2 Initial Conditions,” *ApJ* **542**, pp. 1–8, Oct. 2000.
55. I. Szapudi, “A New Method for Calculating Counts in Cells,” *ApJ* **497**, pp. 16–+, Apr. 1998.
56. I. Szapudi, S. Colombi, and F. Bernardeau, “Cosmic statistics of statistics,” *MNRAS* **310**, pp. 428–444, Dec. 1999.